

Soft x-ray spectroscopic study of the ferromagnetic insulator $V_{0.82}Cr_{0.18}O_2$ L. F. J. Piper,^{*} A. DeMasi, S. W. Cho, A. R. H. Preston, J. Laverock, and K. E. Smith[†]
*Department of Physics, Boston University, 590 Commonwealth Avenue, Boston, Massachusetts 02215, USA*K. G. West, J. W. Lu, and S. A. Wolf
Department of Materials Science, University of Virginia, Charlottesville, Virginia 22904, USA

(Received 8 August 2010; published 1 December 2010)

The chromium-vanadium oxide system $V_{1-x}Cr_xO_2$ ($0.1 < x < 0.2$) displays *both* insulating character in the rutile phase and room-temperature ferromagnetism. A combination of x-ray photoemission spectroscopy, resonant inelastic x-ray scattering, and resonant x-ray emission spectroscopy of the V $L_{3,2}$, O K , and Cr $L_{3,2}$ edges was used to study the electronic structure near the Fermi level of $V_{0.82}Cr_{0.12}O_2$. Our results show that the chromium enters as Cr^{3+} with the d^3 configuration, resulting in the formation of $Cr^{3+}-V^{5+}$ ion pairs, in contrast to the simple Cr^{4+} substitution expected from the end members VO_2 and CrO_2 . The occupied Cr $3d$ orbital is located ~ 2 eV below the Fermi level. Comparison with the parent material VO_2 reveals significant changes in the O $2p$ bandwidth and increased O $2p$ -V $3d$ hybridization in $V_{0.82}Cr_{0.12}O_2$, which are attributed to the reduced atomic spacing upon doping. Two energy loss features due to $d-d^*$ transitions are observed at 0.95 and 1.75 eV in the V L_3 -edge x-ray scattering spectra and are explained in terms of the splitting of the t_{2g} -derived π band.

DOI: [10.1103/PhysRevB.82.235103](https://doi.org/10.1103/PhysRevB.82.235103)

PACS number(s): 71.27.+a, 78.70.En, 71.20.-b, 71.30.+h

I. INTRODUCTION

There is a technological and fundamental interest in early transition-metal oxides, where strong electron-correlation effects give to a variety of ground states (structural, magnetic, and electronic), resulting in rich physics and functionality. Developments in the growth of new alloy compositions and fabrication of nanoscale thin films over the last decade have provided an opportunity to further tailor these properties, and often result in the observation of new phenomena. One such example is the chromium-doped vanadium-oxide system $V_{1-x}Cr_xO_2$ ($0.1 < x < 0.2$) which displays *both* insulating character in the rutile phase and room-temperature ferromagnetism.¹

In its bulk form, pure vanadium dioxide displays an abrupt metal-insulator transition (MIT) at ~ 340 K accompanied by a rutile (D_{4h}) $P4_2/mnm$ (136) to monoclinic (C_{2h}) $P2_1/c$ (12) or M_1 phase transition, along with the formation of nanoscale strongly correlated metal nucleation sites upon the onset of the MIT.² The transition is understood to be driven by the formation and tilting of V-V pairs along the c axis upon going from the metallic rutile phase to the insulating monoclinic phase. In the near-octahedral symmetry of the rutile phase, the V t_{2g} orbitals are split into e_g (π^*) and a_{1g} ($d_{||}$) states, both of which (crucially) overlap the Fermi level. Structurally, the rutile to monoclinic transition corresponds to the dimerization of V-V pairs, which leads to a splitting of the a_{1g} band, and their tilting within the oxygen octahedron, which pushes the e_g band to higher energies and deoccupies it.³ Whether the lattice (Peierls) or electron correlation (Mott-Hubbard) is responsible for driving the subsequent gap at the Fermi level has been hotly debated for many years, but a general consensus has arisen among experiment and theory that both pictures are important, i.e., a Mott-assisted Peierls transition (or vice versa),^{4,5} with structural- and electron-correlation aspects treated on equal footing. It is possible to lower the transition temperature by suitably

straining the c axis⁶ or by chemical substitution of the V^{4+} ions (e.g., electron doping with W, Mo, and Nb), indicating a stabilization of the metallic phase (contrary to the expectations from a purely Peierls perspective). Doping with small concentrations (up to 5%) of Cr^{4+} has a minor effect on conductivity but gives rise to important structural modifications.^{7,8} In particular, the formation of the insulating $C2/m$ (M_2) structure has attracted substantial interest, e.g., Ref. 9, in which only one-half of the V atoms dimerize along the c_R axis and the other one forms zigzag chains of equally spaced atoms.^{7,8} The connection between dopants and structure was first shown for the Cr case by Pouget *et al.* who applied uniaxial stress along the $[110]_R$ direction of *pure* VO_2 samples to obtain the M_2 phase.¹⁰ Recently, the substitution of W was found to induce a similar behavior, but with a biaxial strain on *both* sublattices, with the local rutile environment around the W acting as nucleation sites to destabilize the insulating monoclinic phase and lower the transition temperature.¹¹ The observed insulating and ferromagnetic character of rutile-phase $V_{1-x}Cr_xO_2$ at higher concentrations ($0.1 \leq x \leq 0.2$), that is persistent from 400 K to at least below 100 K, has provided an opportunity to examine further the intimate relationship between structural distortions and electronic structure in vanadium oxides. Here, we build upon the earlier structural, magnetic, and transport measurements of high-quality single crystals of $V_{0.82}Cr_{0.12}O_2$,¹ by employing a combination of x-ray photoemission spectroscopy (XPS), resonant inelastic x-ray scattering (RIXS), and resonant x-ray emission spectroscopy (RXES) at the V $L_{3,2}$, O K , and Cr $L_{3,2}$ edges to provide a complete description of the electronic structure near the Fermi level of $V_{0.82}Cr_{0.18}O_2$ with direct comparison to its parent material VO_2 .

Recent x-ray absorption spectroscopy (XAS) studies at the O K and V $L_{3,2}$ edges of VO_2 have provided new insight into the MIT.^{4,5} Oxygen K XAS corresponds to electron transitions from the occupied O $1s$ level to unoccupied O $2p$

levels. Dipole selection rules ($\Delta l \pm 1$) govern the radiative transition to or from the core level.¹² Thus XAS measurements yield information on the O $2p$ partial density of states (PDOS) above E_F . (The PDOS is the electronic density of states, resolved into orbital angular momentum components). In the case of VO_2 it is possible to use O K -edge XAS to also measure the unoccupied V $3d$, t_{2g} and e_g states that are hybridized with the unoccupied O $2p$ states and study their evolution across the MIT.^{5,13} However, strong atomic (i.e., multiplet) effects exist in the V $L_{3,2}$ -edge ($3d-2p$) XAS due to the large overlap between the core and valence wave functions.¹⁴ As a result, the V $L_{3,2}$ -edge XAS spectrum does not reflect the unoccupied V $3d$ PDOS but can provide information regarding orbital switching across the MIT of bulk VO_2 , as shown by Haverkort *et al.*⁴

In the work reported here, we study both the x-ray absorption process and the corresponding x-ray emission process for each particular absorption edge. In the case of the O K -edge XES we excite above the absorption threshold and measure the fluorescent $2p \rightarrow 1s$ transitions, i.e., the O $2p$ occupied PDOS. In the same manner, exciting the V (and Cr) L_3 -edge XES can also yield information regarding the V(Cr) $3d$ PDOS that can be directly compared with valence-band XPS measurements and calculations. Two additional phenomena can be observed with resonant excitation. First, if the system exhibits core-level shifts due to different chemical bonding or site symmetry, holes can be resonantly created on each core level and the PDOS associated with a particular bond or chemical environment can be measured. This variant is referred to as RXES. The second phenomenon that can appear with resonant excitation are features in the emission spectrum associated with excitations near E_F ; i.e., the incident photon, resonant with a core level, excites an electron-hole pair around E_F and scatters from the system with an energy-loss characteristic energy of the valence excitation. This variant of XES is known as RIXS. RIXS loss features follow the incident photon energy in contrast to PDOS features seen in XES or RXES, which are at a fixed photon energy corresponding to the transition into the core hole. This makes the identification of PDOS and RIXS features in XES spectra straightforward.¹² The RIXS cross section is described by the Kramers-Heisenberg equation and both atomiclike (i.e., crystal-field excitations) and bandlike features can be observed depending on the intersite interactions in the intermediate state of the process. Braicovich *et al.* recently employed V $L_{3,2}$ -edge RIXS to study $d-d^*$ excitations in the insulating monoclinic phase of VO_2 . These excitations are associated with the splitting of the $3d$ states near E_F into occupied $d_{||}$ and unoccupied $d_{||}^*$ and π^* bands.¹⁵ By combining the aforementioned techniques with traditional photoemission spectroscopy we were able to observe significant changes in the O $2p$ bandwidth and increased O $2p$ -V $3d$ hybridization upon doping, which we concluded were linked to the formation of Cr^{3+} - V^{5+} ion pairs and the distortion of the rutile structure. Our results support the original idea by Goodenough and Hong⁷ that the distortion results in two distinguishable oxygen sites and the splitting of the π band (with the $d_{||}$ band totally unoccupied) at these Cr concentrations (i.e., $x > 7\%$). The observed low-energy excitations in the V L_3 -edge RIXS are considered in terms of

t_{2g} $d-d^*$ transitions involving occupied π^* orbital and the unoccupied π^* and $d_{||}^*$ bands.

II. EXPERIMENT

High-quality thin films (200 nm) of $\text{V}_{0.82}\text{Cr}_{0.18}\text{O}_2$ were prepared using the reactive bias target ion-beam deposition and grown upon (0001) sapphire substrates (MTI Crystal) with the b_R axis normal to the surface plane (i.e., c_R axis in the surface plane). The Cr was found to be homogeneously distributed and further details regarding the growth technique and crystalline quality of these films can be found elsewhere.^{1,16} A 100-nm-thick undoped VO_2 film was grown on $\text{TiO}_2(011)$ as a reference sample.¹⁷

The majority of soft x-ray experiments were performed at the undulator beamline X1B at the National Synchrotron Light Source (NSLS), Brookhaven National Laboratory. Complementary RXES experiments were performed on reference VO_2 samples at beamline 7.0.1 at the Advanced Light Source, Lawrence Berkeley National Laboratory. Both beamlines are equipped with spherical grating monochromators and Nordgren-type grazing-incidence spherical grating spectrometers with linear polarization in the horizontal plane. For RIXS measurements, the beamline was set to energy resolutions of 700 meV for the V $L_{3,2}$ and O K edges and 1.1 eV for the Cr $L_{3,2}$ edge, and the emission spectrometer was set to a resolution of 370 meV for the O K edge and V $L_{3,2}$ edges and 600 meV for the Cr $L_{3,2}$ edge. The energy axes were calibrated from Zn metal $L_{3,2}$ emission lines (V $L_{3,2}$ and O K edges) and Cr metal $L_{3,2}$ edges.¹⁸ XAS spectra were recorded in total electron yield (TEY) mode by measuring the sample drain current and were normalized to the current from a reference Au-coated mesh in the incident photon beam. The energy resolution was set at 190 meV for the O K and V $L_{3,2}$ edges and 220 meV for the Cr $L_{3,2}$ edge. The energy scale of the XAS measurements was calibrated using first- and second-order diffraction Ti $L_{3,2}$ edge absorption features of rutile TiO_2 .¹⁹ Additionally XAS in the partial fluorescent yield (PFY) mode were taken of the O K edge. In this case, the XES spectrometer was employed and the count rate over the V $L_{3,2}$ - and O K -edge energy region (490–560 eV) was measured as a function of incident energy with a beamline resolution of 400 meV. All XPS measurements were performed at X1B using a SCIENTA-100 hemispherical electron-energy analyzer; the O $1s$ and V $2p$ core levels were measured with a beamline resolution of better than 450 meV and an instrumental resolution of 400 meV. For the valence-band (VB) XPS, the beamline resolution was better than 200 meV and an instrumental resolution of 160 meV.

Vanadium oxides are extremely sensitive to surface reduction, which can be problematic for surface-sensitive electronic-structure probes such as photoemission, or TEY. Changes in the surface oxidation states of vanadium oxides can be determined from the binding energy of V $2p$ doublet photolines; upon reduction there is a shift of the V $2p_{3/2}$ peak toward lower binding energies.^{20,21} Alternatively, the multiplet structure of the metal $L_{3,2}$ edges (especially vanadium) are also sensitive to the charge state.²² For our reference

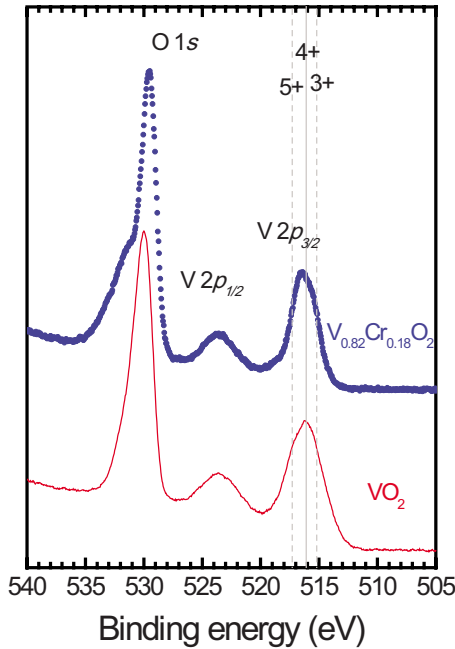


FIG. 1. (Color online) The O $1s$ and V $2p$ XPS of $V_{0.82}Cr_{0.18}O_2$ (blue, upper) and VO_2 (red, lower). The peak energies of the V $2p_{3/2}$ associated with different charge states are also displayed.

material $VO_2(011)$, we were able to prepare atomically clean, well-ordered (2×1) reconstructed surfaces by cycles of Ar^+ -ion bombardment (500 V, 25 mA, 10 min) followed by annealing in an O_2 partial pressure (600 °C, 2×10^{-6} torr, 30 min) cycles with base pressure typically 1×10^{-10} torr. Comparison of the V $2p$ XPS and TEY-mode V $L_{3,2}$ -edge XAS revealed no change in charge state upon cleaning. Unfortunately, the $Cr_{0.18}V_{0.82}O_2$ surfaces were more readily reduced in our experiments with a clear reduction to the V^{3+} charge state in both the V $2p$ XPS and TEY-mode V $L_{3,2}$ -edge XAS (not shown here). As a result, we only present the results from degassed (300 °C for 30 min) $Cr_{0.18}V_{0.82}O_2$ samples where the contamination layer was reduced sufficiently to perform XPS. No difference was noted between as-loaded and degassed samples TEY-mode V $L_{3,2}$ -edge XAS.

III. RESULTS

Figure 1 displays the XPS of the O $1s$ and V $2p$ regions of $V_{0.82}Cr_{0.18}O_2$ and VO_2 . As mentioned previously, care was taken to reduce the contamination layer of $Cr_{0.18}V_{0.82}O_2$ surfaces without affecting the charge state of the vanadium species. As a result, we were unable to prepare atomically clean $Cr_{0.18}V_{0.82}O_2$ surfaces, in contrast to VO_2 . This is evident from the high binding-energy shoulder on the O $1s$ signal (likely due to hydroxyl species) for $Cr_{0.18}V_{0.82}O_2$, which is absent for VO_2 . From comparison with the surface reduction in $V_2O_5(001)$ induced by Ar^+ -ion bombardment reported by Silversmit *et al.*,^{20,21} the V $2p_{3/2}$ photolines of $Cr_{0.18}V_{0.82}O_2$ correspond to a slightly higher oxidation state than V^{4+} (i.e., for VO_2). This suggests that the Cr^{3+} ions rather than Cr^{4+} are incorporated at least within the surface region. The

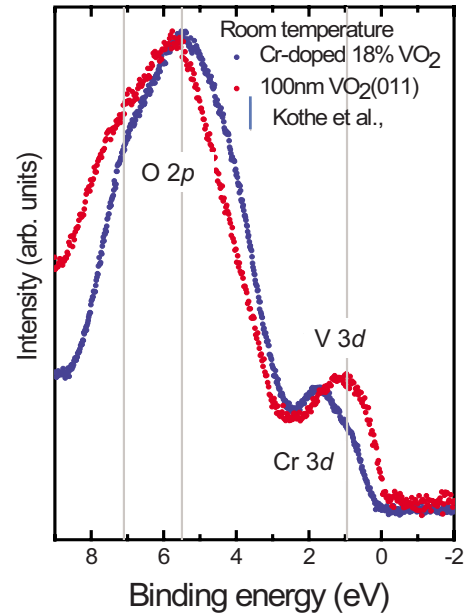


FIG. 2. (Color online) The VB-XPS of $V_{0.82}Cr_{0.18}O_2$ (blue) and VO_2 (red). The vertical lines reflect features of insulating VO_2 reported by Koethe *et al.* (Ref. 5).

shift of 300 meV between the Cr $2p$ core levels associated with Cr^{3+} (Cr_2O_3) and Cr^{4+} (CrO_2) would be difficult to revolve with our energy resolution.²³ Instead, we have employed bulk sensitive Cr $L_{3,2}$ -edge RIXS to determine the charge state, discussed further below.

Figure 2 displays the room-temperature VB-XPS of the two samples measured with incident photon energy of 250 eV. The reference VO_2 is in the insulating phase at room temperature. We note agreement between our spectra with soft x-ray (700 eV) VB-XPS of the insulating phase previously reported by Koethe *et al.*⁵ This is highlighted by vertical lines indicating the O $2p$ and V $3d$ peak energies. The VB-XPS spectrum confirms the insulating character of $V_{0.82}Cr_{0.18}O_2$, in agreement with previous temperature-dependent resistivity measurements.¹ The peak at ~ 0.9 eV is attributed to localized V $3d$ bonding states for both materials. The additional peak at ~ 2 eV observed for $V_{0.82}Cr_{0.18}O_2$ is assigned as the occupied Cr $3d$ orbitals, by comparison with CrO_2 .²⁴ Along with the emergence of the additional Cr $3d$ peak, there is a clear shift of the O $2p$ bonding states toward lower binding energies, compared to VO_2 .

Figure 3(a) displays the room-temperature V $L_{3,2}$ - and O K -edge XAS for $V_{0.82}Cr_{0.18}O_2$ in the TEY mode. Between 513 and 528 eV the V L -edge spectra exhibit a spin-orbit split doublet for the $2p$ states. The absorption band from 513 to 521 eV is derived from the V $2p_{3/2} \rightarrow V 3d$ transition (V L_3) and the one from 521 to 528 eV from the V $2p_{1/2} \rightarrow V 3d$ transition (V L_2). Just above the V L_2 edge at ~ 528 eV, the spectrum in Fig. 3(a) displays the part of the O K XAS spectral weight here originates from O $2p$ states hybridized with crystal-field split V $3d$ states (t_{2g} and e_g). The XAS spectra are similar to insulating phase VO_2 (V^{4+}) (Ref. 4) and metallic phase V_6O_{13} (mixed V^{4+} and V^{5+}).²⁵

The V L_3 -edge resonant emission spectra associated with the fluorescent decay of an occupied V $3d$ electron into the

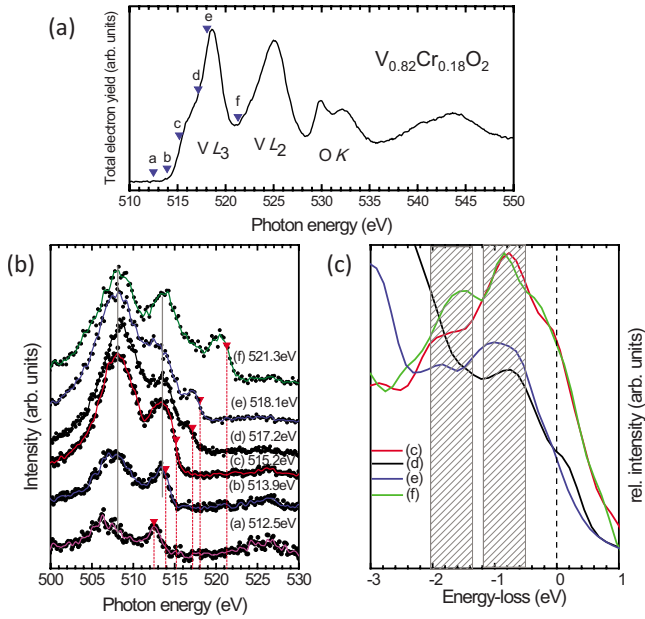


FIG. 3. (Color online) (a) The $V L_{3,2}$ -edge and O K -edge XAS of $V_{0.82}Cr_{0.18}O_2$. The arrows (a)–(f) represent incident energies used to excite the $V L_3$ -edge RIXS/RXES process. (b) The corresponding $V L_3$ -edge RIXS/RXES spectra vertically offset. (c) The enlarged region of RIXS features near the elastic peak (zero energy) plotted on a common energy-loss plot.

empty $V 2p$ core hole following the excitation of $V 2p_{3/2}$ electrons [incident photon energies marked a–f in Fig. 3(a)] are shown in Fig. 3(b). The RXES spectra provide an accurate reflection of the $V 3d$ local PDOS (LPDOS). The $V L_3$ -peak RXES spectra reflect the $V 3d$ LPDOS with two emission peaks at ~ 508 and 513 eV. These peaks are fixed as a function of incident energy (a–f). The separation of peaks agrees well with the separation of the O $2p$ -dominant and $V 3d$ -dominant peaks in the VB-XPS (Fig. 2). In this manner one can consider the peak at ~ 513 eV as associated with states having almost purely $V 3d$ character, and the broader peak at ~ 508 eV reflecting the $V 3d$ states strongly hybridized with the O $2p$ states, as observed for other vanadates.^{25–27} This will be discussed further below.

RIXS measures low-energy excitations (i.e., crystal-field excitations). For the resonant excitations (a–e), the core electrons are promoted into an intermediate (but neutral) state and decay either to the valence excited or ground state. In a $3d$ ion, the scattering path across the $L_{3,2}$ edges is the dipole allowed $2p^6 3d^n \rightarrow 2p^5 3d^{n+1} \rightarrow 2p^6 3d^{n*}$, where n is the ground-state occupation and $*$ indicates an excited state. Figure 3(c) displays the $V L_3$ -edge RIXS/RXES spectra on an energy-loss scale (referenced to the incident photon energy). Fixed energy-loss peaks at ~ 0.95 and ~ 1.75 eV are clearly visible. These are similar (albeit larger in energy) than the $d-d^*$ excitations observed for monoclinic-phase insulating VO_2 reported by Braicovich *et al.*¹⁵ For $V L_{3,2}$ -edge RIXS of VO_2 , $d-d^*$ transitions between the t_{2g} -derived occupied $d_{||}$ and the unoccupied π^* and $d_{||}^*$ bands were observed, the center of which are 0.85 eV (π^*) and 1.5 eV ($d_{||}^*$). However, it should be noted that despite the proximity in energy of our excitations to those of Ref. 15 the different crystal-field split-

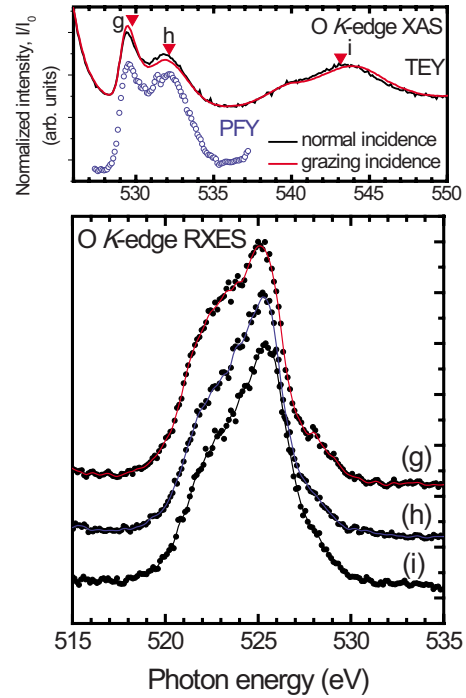


FIG. 4. (Color online) (Top) The O K -edge XAS $V_{0.82}Cr_{0.18}O_2$. The arrows (g)–(i) represent incident energies used to excite RXES process. (Bottom) The corresponding O K -edge RXES spectra, vertically offset.

ting of pure, monoclinic VO_2 , and the near-rutile structure of the $V_{0.82}Cr_{0.18}O_2$ (reported elsewhere Ref. 28) under consideration here preclude a similar origin for the loss features observed for $V_{0.82}Cr_{0.18}O_2$ and will be discussed in detail.

Room-temperature O K -edge (a) XAS and (b) RXES spectra are shown in Fig. 4. In addition to the TEY-mode XAS we also include the more bulk-sensitive PFY XAS, which displays the same spectral shape for the TEY mode and rules out possible surface effects. O K -edge XAS is a powerful tool for investigating the unoccupied transition metal (TM) $3d$ band due to the covalent mixing of the TM $3d$ -O $2p$ orbitals.²⁹ The vanadium (and chromium) $3d$ states are split by the octahedral crystal field into upper e_g and lower t_{2g} levels. The empty $V e_g$ orbitals form an antibonding band and the t_{2g} levels are located near the Fermi level. As a result, the O K -edge XAS peaks (g) and (h) reflect the unoccupied O $2p$ states hybridized with crystal-field split $V 3d$, t_{2g} and e_g states (and to a lesser extent the corresponding Cr $3d$ states). Meanwhile, the broad continuum 540 – 550 eV reflects the O $2p$ - $V(Cr)4s,p$ hybridized states. In the metallic phase of VO_2 , the partially filled $d_{||}$ and empty π^* bands derived from the t_{2g} electrons overlap. Below the MIT (in the monoclinic phase), the splitting of the $d_{||}^*$ band and 0.5 eV energetic up-shift of the π^* can be directly observed from the O K -edge XAS.^{5,13} The $d_{||}^*$ peak can be seen with $E || c_R$ polarization only, since mainly the O $2p_z$ orbitals (with z along c) have sufficient hybridization with the $d_{||}$ state.⁵ The angular dependence of TEY XAS of $V_{0.82}Cr_{0.18}O_2$ revealed only a slight variation in the relative intensities of the t_{2g} - and e_g -related peaks with grazing (i.e., E parallel to the b_R axis) and perpendicular (i.e., E parallel to the a_R - c_R plane incidence geometry).

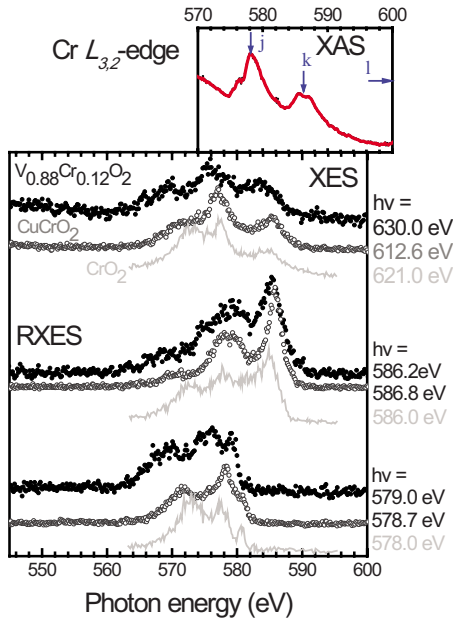


FIG. 5. (Color online) (Top) The Cr $L_{3,2}$ -edge XAS $V_{0.82}Cr_{0.12}O_2$. The arrows (j)–(l) represent incident energies used to excite RXES process. (Bottom) The corresponding Cr $L_{3,2}$ -edge RXES spectra, vertically offset. Reference Cr $L_{3,2}$ -edge RIXS spectra (with similar excitation energies) for (dark gray empty circles) $CuCrO_2$ (Ref. 30) and (light gray lines) CrO_2 (Ref. 31) are also displayed for direct comparison.

Returning to the RXES data in Fig. 4, the excitation energy (i) is well-above threshold and reflects the O $2p$ LPDOS. The spectral shape between photon energies 522–526 eV is in good agreement with the predominantly O $2p$ region of the VB-XPS (binding energies 8–4 eV) in Fig. 2. Furthermore, the weak shoulder at ~ 528 eV can be associated with O $2p$ hybridization with Cr $3d$ and V $3d$ states, from comparison with the VB-XPS and analogy with similar vanadium oxides, e.g., V_6O_{13} .²⁵ The spectral difference between the RXES spectra (g) and (h) are then associated with the occupied LPDOS O $2p$ hybridized with t_{2g} and e_g states, respectively.

The Cr $L_{3,2}$ -edge RXES and corresponding XAS spectra are displayed in Fig. 5(a), along with reference Cr L -edge spectra (with similar excitation energies) for $CuCrO_2$ (Cr^{3+}) (Ref. 30) and CrO_2 (Cr^{4+}).³¹ It is difficult to obtain Cr $L_{3,2}$ -edge emission data with good signal-to-noise ratio in

chromium oxides due to simultaneously exciting the above-threshold O K edge (and the V $L_{3,2}$ edge for this compound) combined with the high efficiency of its Auger decay process. Nevertheless, we obtain greater agreement with our previous studies of $CuCrO_2$ (Cr^{3+}),³⁰ than for CrO_2 (Cr^{4+}).³¹ This is in keeping with the aforementioned V $2p$ XPS (Fig. 1) and would suggest that the chromium enters as Cr^{3+} with the d^3 configuration, resulting in the formation of $Cr^{3+}-V^{5+}$ ion pairs, as proposed by Goodenough and Hong for $V_{1-x}Cr_xO_2$ ($0 < x \leq 0.20$).⁷

IV. DISCUSSION

Our experimental results provide evidence for the formation of $V^{5+}-Cr^{3+}$ pairs, in contrast to the simple Cr^{4+} substitution expected from the end members VO_2 and CrO_2 . Such basic characterization may play an important role in understanding the insulating and ferromagnetic character of $V_{1-x}Cr_xO_2$ ($0.1 \leq x \leq 0.2$). A recent theoretical attempt to determine the electronic and magnetic properties of rutile $V_{1-x}Cr_xO_2$ ($0.1 \leq x \leq 0.2$) by Williams *et al.* calculated its electronic structure using density-functional theory in the generalized gradient approximation and with empirical on-site Coulomb correlations (GGA+ U). Within these approximations they concluded a ferromagnetic half-metallic ground state with a magnetic moment of 1 μ_B per Cr ion substituted based on the +4 charge state of both the V and Cr atoms.³² Clearly the experimentally observed mixed charge state of the vanadium ions could affect these calculations. For instance, the Li insertion of $Li_xV_6O_{13}$ ($0 \leq x \leq 6$) results in electronic transfer to the vanadium ions (i.e., reducing the vanadium) and modifying the valence-band region.³³ We have chosen to investigate the effect of the mixed valence state by comparing our V L_3 RXES spectrum of $V_{0.82}Cr_{0.18}O_2$ [in Fig. 3(b)] with results from our reference insulating-phase VO_2 . Figure 6(a) displays the comparison. Apart from the intensity of the elastic peak, the greatest difference between the two spectra is the reduction in the pure V $3d$ PDOS (~ 513 eV) due to electronic transfer from the vanadium sites following the incorporation of Cr. The observed trend in spectral weight between the peak of purely V $3d$ character (~ 513 eV) and that reflecting the V $3d$ states strongly hybridized with the O $2p$ states (~ 508 eV) between $V_{0.82}Cr_{0.18}O_2$ and VO_2 is in agreement with the lithiation of $Li_xV_6O_{13}$ ($0 \leq x \leq 6$) with a similar change in

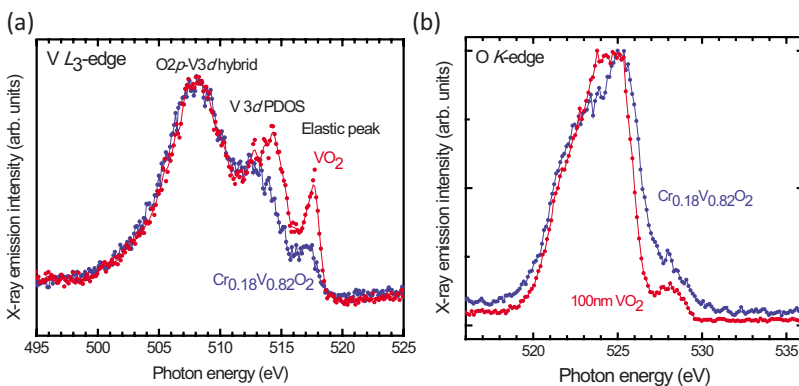


FIG. 6. (Color online) The (a) V L_3 - and (b) O K -edge peak RXES spectra of $V_{0.82}Cr_{0.12}O_2$ (blue) and VO_2 (red).

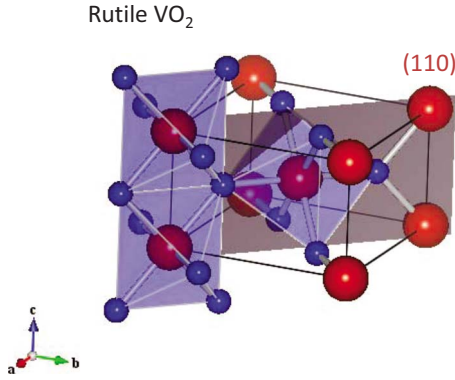


FIG. 7. (Color online) (a) A schematic representation of the rutile VO_2 structure with the oxygen octahedron (small, blue spheres) around the edge and center vanadium ions (large, red spheres) shown, along with the (110) plane (shaded plane).

effective charge state.³³ For $\text{Li}_x\text{V}_6\text{O}_{13}$, the spectral variation was considered to reflect the reduction the degree of V $3d$ -O $2p$ hybridization due to the decrease in the overlap of the V $3d$ -O $2p$ orbitals associated with the structural distortion induced by the Li insertion.³³ Likewise, one would expect an accompanying change in the O K -edge RXE spectra. Figure 6(b) displays the comparison between the O K -edge RXE spectra of $\text{V}_{0.82}\text{Cr}_{0.18}\text{O}_2$ and VO_2 excited on the t_{2g} state, i.e., excitation (g) in Fig. 4. We see increased O $2p$ bandwidth compared to VO_2 , also seen for the VB-XPS in Fig. 2.

Most recently, Booth and Casey reported an extended x-ray absorption spectroscopy fine-structure (EXAFS) study of pure and W-doped VO_2 where they observed significant expansion in the $[110]_R$ and $[\bar{1}10]_R$ directions across the phase transition from the insulating low-temperature phase to the metallic high-temperature phase.¹¹ Chromium doping is known to result in a reduction in the spacing of the (110) planes, which is linear with the Cr concentration up to at least $x=0.20$.²⁸ The distortion of the rutile crystal is likely responsible for the increased V $3d$ -O $2p$ overlap, which, in turn, stabilizes the insulating phase. Following W doping where the spacing of the (110) planes are increased and the MIT significantly lowered,²⁸ one would expect an opposite trend between the alloy and parent material to that in Fig. 6. Although no RXES studies exist for $\text{V}_{1-x}\text{W}_x\text{O}_2$ at the desired

concentrations (i.e., $0.1 \leq x \leq 0.2$), V $L_{3,2}$ - and O K -edge RXES data have been published for $\text{V}_{1-x}\text{Mo}_x\text{O}_2$ ($x=0.8, 0.18$) which displays similar properties to W-doped VO_2 .²⁷ An opposite trend (for both edges) is observed for the Mo-doped compared to our Cr-doped case, i.e., reduced V $3d$ -O $2p$ overlap is reported for the Mo-doped case.²⁷ These results provide important insight into the role of the V $3d$ -O $2p$ hybridization in contributing to the MIT mechanism of the parent material.

Figure 7 displays a schematic of the rutile structure with the octahedral oxygen ions for certain edge and center vanadium ions, using VESTA software.³⁴ As mentioned previously, the substitution of chromium ($0.1 < x < 0.2$) for vanadium reduces the spacing of the (110) planes.²⁸ As a result, two distinct oxygen sites emerge due to the difference in the distortion of the equatorial and apex oxygen ions around the edge and center vanadium ions. The V-O distances shrink for the apex and equatorial oxygen in the atoms around the center and edge vanadium ions, respectively. Likewise, the remaining V-O distances increase from their original separations. As a result, the oxygen sites along the $(1\bar{1}0)$ and (110) planes differ. It should be noted that this distortion is similar to the proposed M_4 $P2/m$ monoclinic phase proposed by Goodenough and Hong for Cr-doping greater than 6%;⁷ corresponding to a weak distortion of the rutile structure, in contrast with the strong dimerizing distortions of either the M_1 or M_2 phase. Additional structural studies of $\text{V}_{1-x}\text{Cr}_x\text{O}_2$ are required and currently limit our discussion in terms increased V $3d$ -O $2p$ due to the aforementioned distorted rutile structure.

Figure 8 displays a schematic representation of the energetic levels of the V $3d$ and O $2p$ states for Cr-doped VO_2 above and below the MIT proposed by Goodenough and Hong.⁷ In their two-band model for Cr-doped VO_2 ($0 < x < 0.2$) the V $3d$ orbitals are first stabilized within the orbitally nondegenerate $d_{||}$ band at low Cr concentrations and then stabilized within the twofold degenerate π^* band at higher concentrations ($0.08 < x < 0.20$). In the low-temperature regime, the lattice distortion (i.e., rutile to monoclinic) concentrates the electrons within the most stable band with an insulating phase formed by the splitting of the band. Their model also considered the formation of Cr^{3+} - V^{5+} pairs (up to $x=0.20$ after which the $\text{V}^{5+}\text{Cr}^{3+}\text{O}_2$ phase should segregate out) and how the π^* band is susceptible to changes

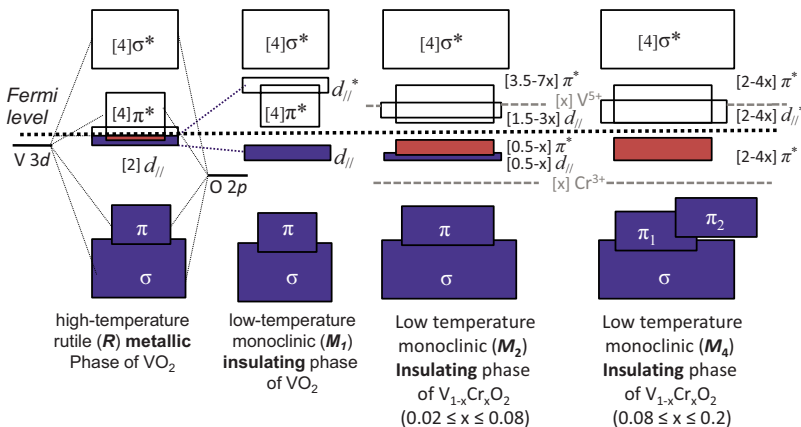


FIG. 8. (Color online) A schematic representation of the molecular orbitals near the Fermi level for rutile R ($P4_2/mmm$) and monoclinic M_1 ($P2_1/c$), M_2 ($C2/m$), and M_4 ($P2/m$) phases of VO_2 and Cr-doped VO_2 proposed by Goodenough and Hong (Ref. 7).

in the V-O separation (i.e., c_R/a_R ratio). Figure 8 displays the molecular-orbital description of the rutile R ($P4_2/mnm$) and monoclinic M_1 ($P2_1/c$), M_2 ($C2/m$), and M_4 ($P2/m$) phases proposed by Goodenough and Hong.⁷ In the M_4 phase, we have displayed the insulating character arising from the splitting of the π^* band. This is a possibility discussed by Goodenough and Hong and we consider the most likely scenario considering the observed insulating character of our $V_{0.82}Cr_{0.18}O_2$ samples (for $T < 400$ K). Our x-ray studies of $V_{0.82}Cr_{0.18}O_2$ have revealed evidence of $Cr^{3+}-V^{5+}$ ion pairs and increased V $3d-O$ $2p$ hybridization [likely associated with reduced spacing of the $(110)_R$ planes],²⁸ consistent with the insulating M_4 phase of the two-band model. Referring to the energy-loss features within the V $L_{3,2}$ -edge RIXS (Fig. 3) it is unlikely that the same description for the M_1 phase would be valid for our 18% doped case despite the similar energies to insulating VO_2 . Instead, it is more likely that the increased V $3d-O$ $2p$ hybridization is responsible for splitting the π^* band with the lack of V-V pairing along the c_R axis resulting in an empty $d_{||}^*$ band, as shown in Fig. 8 for the insulating M_4 phase.⁷ As a result, we consider the low-energy excitations in the V L_3 -edge RIXS in Fig. 3 to be related to t_{2g} $d-d^*$ transitions involving occupied π^* bands to the unoccupied π^* and $d_{||}^*$ bands as depicted in Fig. 8 for the insulating M_4 phase.

V. CONCLUSION

We have employed a combination of soft x-ray spectroscopic techniques to investigate the electronic structure near

the Fermi level of ferromagnetic insulating $V_{0.82}Cr_{0.18}O_2$. We have built upon earlier structural, magnetic, and transport measurements and have determined that the chromium substitutes as Cr^{3+} with the Cr $3d$ bands lying ~ 2 eV below the Fermi level. The formation of $V^{5+}-Cr^{3+}$ pairs and location of the Cr $3d$ bands should be considered within any explanation of the observed ferromagnetic character. The insulating phase of $V_{0.82}Cr_{0.18}O_2$ is considered a result of increased V $3d-O$ $2p$ hybridization related to the reduced (110) spacing due to Cr substitution and provides further insight into the MIT mechanism of VO_2 .

ACKNOWLEDGMENTS

The Boston University (BU) program is supported in part by the Department of Energy under Contract No. DE-FG02-98ER45680. The University of Virginia (UVa) gratefully acknowledges funding from DARPA through ARO under Grant No. W911NF-08-1-0283. The Advanced Light Source is supported by the Director, Office of Science, Office of Basic Energy Sciences, of the U.S. Department of Energy under Contract No. DE-AC02-05CH11231. Use of the National Synchrotron Light Source, Brookhaven National Laboratory, was supported by the U.S. Department of Energy, Office of Science, Office of Basic Energy Sciences, under Contract No. DEAC02-98CH10886.

*Present address: Department of Physics, Applied Physics and Astronomy, Binghamton University, Binghamton, NY 13902-6000, USA.

†ksmith@bu.edu

¹K. G. West, J. Lu, L. He, D. Kirkwood, W. Chen, T. P. Adl, M. S. Osofsky, S. B. Qadri, R. Hull, and S. A. Wolf, *J. Supercond. Novel Magn.* **21**, 87 (2008).

²M. M. Qazilbash, M. Brehm, B.-G. Chae, P.-C. Ho, G. O. Andreev, B.-J. Kim, S. J. Yun, A. V. Balatsky, M. B. Maple, F. Keilmann, H.-T. Kim, and D. N. Basov, *Science* **318**, 1750 (2007).

³J. B. Goodenough, *J. Solid State Chem.* **3**, 490 (1971).

⁴M. W. Haverkort, Z. Hu, A. Tanaka, W. Reichelt, S. V. Streltsov, M. A. Korotin, V. I. Anisimov, H. H. Hsieh, H.-J. Lin, C. T. Chen, D. I. Khomskii, and L. H. Tjeng, *Phys. Rev. Lett.* **95**, 196404 (2005).

⁵T. C. Koethe, Z. Hu, M. W. Haverkort, C. Schüßler-Langeheine, F. Venturini, N. B. Brookes, O. Tjernberg, W. Reichelt, H. H. Hsieh, H.-J. Lin, C. T. Chen, and L. H. Tjeng, *Phys. Rev. Lett.* **97**, 116402 (2006).

⁶Y. Muraoka and Z. Hiroi, *Appl. Phys. Lett.* **80**, 583 (2002).

⁷J. B. Goodenough and H. Y. P. Hong, *Phys. Rev. B* **8**, 1323 (1973).

⁸M. Marezio, B. Mcwhan, P. D. Dernier, and J. P. Remeika, *Phys. Rev. B* **5**, 2541 (1972).

⁹V. Eyert, *Ann. Phys.* **11**, 650 (2002).

¹⁰J. P. Pouget, H. Launois, J. P. Dhaenens, P. Merenda, and T. M.

Rice, *Phys. Rev. Lett.* **35**, 873 (1975).

¹¹J. M. Booth and P. S. Casey, *Phys. Rev. Lett.* **103**, 086402 (2009).

¹²A. Kotani and S. Shin, *Rev. Mod. Phys.* **73**, 203 (2001).

¹³M. Abbate, F. M. F. deGroot, J. C. Fuggle, Y. J. Ma, C. T. Chen, F. Sette, A. Fujimori, Y. Ueda, and K. Kosuge, *Phys. Rev. B* **43**, 7263 (1991).

¹⁴F. M. F. de Groot, *Coord. Chem. Rev.* **249**, 31 (2005).

¹⁵L. Braicovich, G. Ghiringhelli, L. H. Tjeng, V. Bisogni, C. Dallera, A. Piazzalunga, W. Reichelt, and N. B. Brookes, *Phys. Rev. B* **76**, 125105 (2007).

¹⁶K. G. West, J. W. Lu, J. Yu, D. Kirkwood, W. Chen, Y. H. Pei, J. Claassen, and S. A. Wolf, *J. Vac. Sci. Technol. A* **26**, 133 (2008).

¹⁷J. W. Lu, K. G. West, and S. A. Wolf, *Appl. Phys. Lett.* **93**, 262107 (2008).

¹⁸*X-Ray Data Booklet*, edited by A. C. Thompson, D. Attwood, E. Gullikson, M. Howells K.-J. Kim, J. Kirz, J. Kortright, I. Lindau, P. Pianetta, A. Robinson, J. Scofield, J. Underwood, D. Vaughan, G. Williams, and H. Winick (Lawrence Berkeley National Laboratory, Berkeley, CA, 2001).

¹⁹X. Chen, P.-A. Glans, X. Qiu, S. Dayal, W. D. Jennings, K. E. Smith, C. Burda, and J.-H. Guo, *J. Electron Spectrosc. Relat. Phenom.* **162**, 67 (2008).

²⁰G. Silversmit, D. Depla, H. Poelman, G. B. Marin, and R. De Gryse, *J. Electron Spectrosc. Relat. Phenom.* **135**, 167 (2004).

²¹G. Silversmit, D. Depla, H. Poelman, G. B. Marin, and R. De

- Gryse, *Surf. Sci.* **600**, 3512 (2006).
- ²²G. Cressey, C. M. B. Henderson, and G. Vanderlaan, *Phys. Chem. Miner.* **20**, 111 (1993).
- ²³H. A. Bullen and S. J. Garrett, *Chem. Mater.* **14**, 243 (2002).
- ²⁴T. Tsujioka, T. Mizokawa, J. Okamoto, A. Fujimori, M. Nohara, H. Takagi, K. Yamaura, and M. Takano, *Phys. Rev. B* **56**, R15509 (1997).
- ²⁵T. Schmitt, L.-C. Duda, M. Matsubara, M. Mattesini, M. Klemm, A. Augustsson, J.-H. Guo, T. Uozumi, S. Horn, R. Ahuja, A. Kotani, and J. Nordgren, *Phys. Rev. B* **69**, 125103 (2004).
- ²⁶T. Schmitt, L.-C. Duda, A. Augustsson, J.-H. Guo, J. Nordgren, J. E. Downes, C. McGuinness, K. E. Smith, G. Dhalenne, A. Revcolevschi, M. Klemm, and S. Horn, *Surf. Rev. Lett.* **9**, 1369 (2002).
- ²⁷T. Schmitt, L.-C. Duda, M. Matsubara, A. Augustsson, F. Trif, J.-H. Guo, L. Gridneva, T. Uozumi, A. Kotani, and J. Nordgren, *J. Alloys Compd.* **362**, 143 (2004).
- ²⁸M. Pan, H. M. Zhong, S. W. Wang, J. Liu, Z. F. Li, X. S. Chen, and W. Lu, *J. Cryst. Growth* **265**, 121 (2004).
- ²⁹F. M. F. de Groot, M. Grioni, J. C. Fuggle, J. Ghijsen, G. A. Sawatzky, and H. Petersen, *Phys. Rev. B* **40**, 5715 (1989).
- ³⁰T. Arnold, D. J. Payne, A. Bourlange, J. P. Hu, R. G. Egdell, L. F. J. Piper, L. Colakerol, A. De Masi, P.-A. Glans, T. Learmonth, K. E. Smith, J. Guo, D. O. Scanlon, A. Walsh, B. J. Morgan, and G. W. Watson, *Phys. Rev. B* **79**, 075102 (2009).
- ³¹E. Z. Kurmaev, A. Moewes, S. M. Butorin, M. I. Katsnelson, L. D. Finkelstein, J. Nordgren, and P. M. Tedrow, *Phys. Rev. B* **67**, 155105 (2003).
- ³²M. E. Williams, W. H. Butler, C. K. Mewes, H. Sims, M. Chshiev, and S. K. Sarker, *J. Appl. Phys.* **105**, 07E510 (2009).
- ³³T. Schmitt, A. Augustsson, J. Nordgren, L. C. Duda, J. Howing, T. Gustafsson, U. Schwingenschlogl, and V. Eyert, *Appl. Phys. Lett.* **86**, 064101 (2005).
- ³⁴M. Momma and F. Izumi, *J. Appl. Crystall.* **41**, 653 (2008).